Lifetimes and structures of low-lying negative-parity states of ^{209}Po

V. Karayonchev,[1] M. Stoyanova,[2] G. Rainovski,[2,*] J. Jolie,[1] A. Blazhev,[1] M. Djongolov,[2] A. Esmaylzadeh,[1] C. Fransen,[1] K. Gladnishki,[2] L. Knafla,[1] D. Kocheva,[2] L. Kornwebel,[1] J.-M. Régis,[1] G. De Gregorio,[3,4] and A. Gargano[4]

[1]*Institut für Kernphysik, Universität zu Köln, 50937 Köln, Germany*
[2]*Faculty of Physics, St. Kliment Ohridski University of Sofia, 1164 Sofia, Bulgaria*
[3]*Dipartimento di Matematica e Fisica, Università degli Studi della Campania "Luigi Vanvitelli", I-81100 Caserta, Italy*
[4]*INFN Sezione di Napoli, IT-80126 Napoli, Italy*

(Received 24 September 2020; revised 14 February 2021; accepted 17 March 2021; published 5 April 2021)

The $5/2_1^-$, $9/2_1^-$, and $11/2_1^-$ states in ^{209}Po were populated in the β decay of ^{209}At and their lifetimes measured using the electronic γ-γ fast timing technique. The lifetime of the $9/2_1^-$ state is measured for first time. The lifetime of the $5/2_1^-$ is measured to be shorter than the value adopted in the literature while the lifetime of the $11/2_1^-$ state agrees well with the previous measurement. In order to get deeper insight into the structure of the states, a shell-model calculation was carried out adopting a microscopic effective interaction derived from the realistic CD-Bonn potential. The comparison between theoretical and experimental data for the low-lying negative-parity states of ^{209}Po supports the reliability of the predicted wave functions, which are found to be dominated by the coupling of a neutron hole to the yrast states of ^{210}Po. However, it also points to the important role played by minor wave-function components in describing the reduced electromagnetic strengths, suggesting the need of additional configuration mixing for achieving a better quantitative agreement.

DOI: 10.1103/PhysRevC.103.044309

I. INTRODUCTION

One of the main tasks of modern nuclear structure studies is to seek a comprehensive description of nuclei by simultaneously explaining the rich variety of single-particle and collective phenomena they exhibit. In this regard, it is of particular interest to understand the development of collectivity starting from microscopic degrees of freedom.

A successful framework for microscopic nuclear structure calculations is the shell model, which is based on the assumption that nucleons move independently in a central mean field with a strong spin-orbit term giving rise to the observed shell structure and the corresponding magic numbers [1,2]. Within this model the valence nucleons external to the filled shells interact through the two-body residual interaction (the part of the interaction that is not absorbed into the central potential), which induces a mixing of different configurations. It is well known that the proton-neutron component of the residual interaction tends to drive collective behaviors, and collectivity emerges when this component, which increases with the number of valence protons and neutrons [3], overcomes the pairing interaction [4]. In this context, the evolution of the nuclear states with the number of valence nucleons from single-particle configurations towards multiconfigurational mixture is a matter of great relevance, which may give important information on the properties of the interaction in nuclear medium.

The initial step in addressing this question is to understand the structure of low-lying states of nuclei in the vicinity of shell closures. In fact, nuclei with only few valence protons and neutrons particles (or holes) provide a suitable ground for testing and tuning residual interactions used in the shell-model calculations. They can be particularly useful when interactions are derived within a microscopic approach from realistic nucleon-nucleon potentials, which do not contain free parameters fixed to reproduce experimental data.

The nuclei in the vicinity of the doubly magic nucleus ^{208}Pb have attracted significant interest over the years. In particular, many shell-model calculations have been performed in this region [5–14], motivated by the fact that ^{208}Pb is considered to be a good closed core [5]. It has to be stressed, however, that most of these studies are focused on semimagic lead nuclei or on semimagic $N = 126$ isotones [5,7–11]. Furthermore, in the cases where open-shell nuclei are considered, shell-model calculations are based on empirical interactions [6] and usually focused on the structure of the high-spin isomers [8]. As a matter of fact, the nature of low-spin states of nuclei in the vicinity of ^{208}Pb is still poorly understood, as it was noticed long ago in Ref. [15]. This is due partially to the lack of experimental data, especially on the electromagnetic transition rates. For example, the yrast states of even-even polonium isotopes are thought to be built on the $\pi(h_{9/2})^2$ configuration. This is in agreement with the available experimental data for the 8_1^+ and 6_1^+ states which can be well described in the framework of the shell model with phenomenological interactions [16,17]. However, even in ^{210}Po, where all transition strengths for the yrast states

*rig@phys.uni-sofia.bg

are experimentally well known [18], no consistent description which includes the $B(E2; 2_1^+ \rightarrow 0_1^+)$ exists [11,18]. For ^{208}Po no experimental data on the $E2$ transitions strengths from the 4_1^+ and 2_1^+ states are available, while in ^{204,206}Po there are experimental indications that the 4_1^+ and 2_1^+ states are already of collective nature [19].

To fill the gap in the evolution between the states of single-particle seniority-type character in ^{210}Po and those of collective nature in ^{204,206}Po, we have studied the low-lying negative-parity states of ^{209}Po. The properties of these states may provide information on the increased collectivity with respect to ^{210}Po as it has been demonstrated recently in the case of ^{129}Sb by observing total electric quadrupole strength significantly larger than in the ^{128}Sn core [20].

The ^{209}Po nucleus has been studied extensively in the past mainly through the electron-capture decay of ^{209}At (see Refs. [21,22], and references therein). Therefore, its level scheme is well established with the spin-parity assignment of the states based mostly on measured electron conversion coefficients [21,22]. In particular, the $17/2_1^-$ isomeric state at 1472 keV has been discovered by Yamazaki and Matthias [23] and its lifetime has been measured precisely by Hüsser *et al.* [24], while the lifetimes of the $5/2_1^-$, the $13/2_1^-$, and the $11/2_1^-$ states have been reported in Ref. [21]. Alpsten *et al.* [21] have interpreted these results in the framework of semirealistic shell-model calculations [25], which suggest that the low-lying negative-parity states of ^{209}Po arise from a weak coupling of a single neutron hole to the excited states of ^{210}Po. This interpretation is in overall agreement with the available experimental data on the magnetic dipole moments [24] and the electric quadrupole moments [26] of the isomeric $13/2_1^-$ and $17/2_1^-$ states. However, all previous studies [21–24] also suggest that contributions of minor components in the wave functions of the low-lying negative-parity states of ^{209}Po may play an important role, especially for the description of the electromagnetic properties.

To clarify further the role of the configuration mixing in the structure of low-lying negative parity states of ^{209}Po, more experimental data on electromagnetic transition strengths for states other than the isomeric ones are needed. Moreover, the comparison with the theoretical results would also provide a good test for the realistic interactions used in shell-model calculations. However, the lifetimes of these states are expected to be in order of few tens of picoseconds and their precise determination has not been possible in the past.

Nowadays, with the development of the ultrafast timing technique for γ-ray coincidence spectroscopy [27] which is based on fast $LaBr_3$(Ce) scintillator detectors with high energy resolution [28], such measurements have become possible. It is the purpose of the present study to measure the lifetimes of the the low-lying negative-parity states of ^{209}Po by utilizing the electronic γ-γ fast timing technique and thus to provide data for testing shell-model calculations based on a realistic interaction.

II. EXPERIMENT

The experiment was performed at the FN-Tandem facility of the University of Cologne. The isotope ^{209}Po was populated after the successive α and electron capture (e.c.) decay of ^{213}Fr which was produced in the ^{206}Pb(^{11}B, $4n$)^{213}Fr fusion-evaporation reaction at a beam energy of 56 MeV. The target consists of a ^{206}Pb foil with a thickness of 14.5 mg/cm^2 on a 130 mg/cm^2 gold backing, the latter being used to stop the beam in order to prevent further reactions in the reaction chamber. The γ rays were detected by a mixed array consisting of 8 HPGe detectors and 12 LaBr scintillators mounted at the Cologne HORUS spectrometer. To suppress the Compton background, six of the LaBr detectors were placed inside bismuth-germanate oxide (BGO) anti-Compton shields. The other LaBr detectors had lead shields to suppress background events associated with scattered γ rays. The time differences of every unique combination of LaBr detectors were recorded using time to amplitude converters (TAC) applying the multiplexed-start and multiplexed-stop electronics setup [29]. The target was activated for a period of 90 h at an average beam current of 1.8 pnA. Afterwards, the decay data were acquired off-beam for a period of 100 h. The detector energy signals and the TAC amplitudes were recorded without triggers in a list-mode format. These data were used in the following analysis.

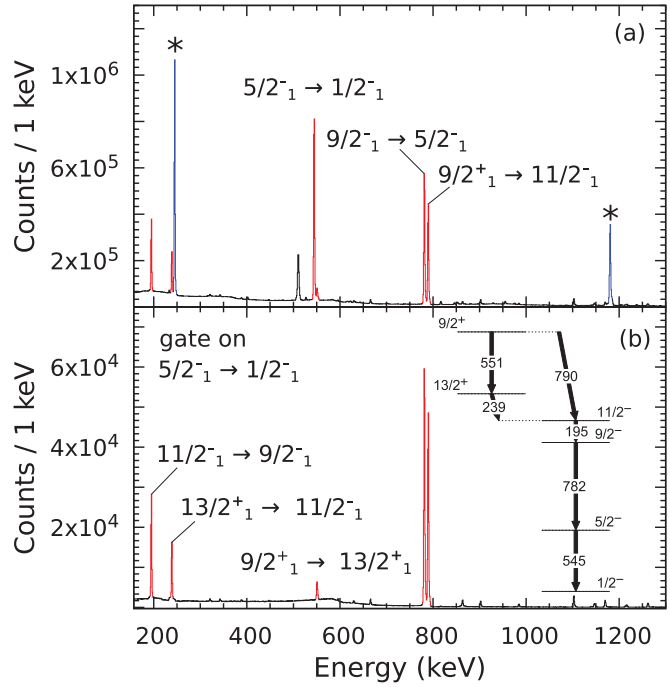

FIG. 1. (a) The full projections of off-beam HPGe-HPGe coincidence data. (b) γ spectrum in coincidence with the $5/2_1^- \rightarrow 1/2_1^-$ transition in ^{209}Po, together with a level scheme of ^{209}Po populated in the e.c. decay of ^{209}At. Transitions belonging to the ^{209}Po are indicated and colored in red. Transitions belonging to ^{210}Po are indicated with an asterisk and colored in blue.

The full projection of HPGe-HPGe coincidence data is displayed in Fig. 1(a). The α decay of ^{213}Fr [$T_{1/2} = 34.14(6)$ s] leads almost exclusively [99.44(5)%] [30] to the ground state ($J^\pi = 9/2^-$) of ^{209}At. ^{209}At decays [$T_{1/2} = 5.42(5)$ h] mainly via electron capture [95.9(5)%] [31] to excited states of ^{209}Po. The γ rays from the decays of these states, are delineated in

red in Fig. 1(a). The transitions in blue are from the decays of the excited states of ^{210}Po which is produced in a similar way from the $3n$ channel of the fusion-evaporation reaction. All γ rays, observed in coincidence with the $5/2^-_1 \rightarrow 1/2^-_{1(\text{g.s.})}$ transition in ^{209}Po [cf. Fig. 1(b)], are from known transitions in ^{209}Po [31]. A partial level scheme of ^{209}Po summarizing the observed γ transitions and their coincidence relationship is shown in the inlay of Fig. 1(b).

The lifetimes were extracted using the fast-timing technique by applying the generalized centroid difference (GCD) method [32]. In this analysis, an asymmetric timing of the γ-γ fast-timing setup is considered. In this case for a given feeder-decay combination of a certain state two independent time-difference spectra are generated. When a feeding transition provides the start signal and the decay transition provides the stop signal, the delayed spectrum is produced. Conversely, when the decay transition provides the start signal and the feeding transition the stop signal, the antidelayed spectrum is produced. In the case where no background is present, the centroids of the delayed and the antidelayed time distributions are shifted by two times the mean lifetime τ of the state plus an energy-dependent time-walk characteristics of the setup, dubbed prompt response difference (PRD) [33]:

$$C_d - C_a = \Delta C = 2\tau + \text{PRD}. \tag{1}$$

Here, C_d and C_a are the centroids of the delayed antidelayed time distributions. The PRD describes the combined mean time-walk characteristics of the fast-timing setup. Its energy dependence is determined by a standard calibration procedure using a ^{152}Eu source [33]. By selecting a feeder-decay combination of a state with a known lifetime the delayed and the antidelayed time-difference spectra are generated. By measuring the centroid difference ΔC and using Eq. (1) the PRD is obtained. The data points are fitted with the function [33]:

$$\text{PRD}(E_\gamma) = \frac{a}{\sqrt{E_\gamma + b}} + cE_\gamma + d. \tag{2}$$

The evolution of the standard deviation (σ) of the fitted PRD curve as a function of energy was derived from the evaluation of the contrivance matrix as suggested in Ref. [27]. It varies from 7 ps at 195 keV down to below 2 ps at higher energies. The result of the fit is presented in Fig. 2.

When extracting the lifetimes triple HPGe-LaBr-LaBr coincidences were used. The additional HPGe gate allows a γ cascade to be selected precisely, reducing the influence of unwanted transitions. In addition, the peak to background ratio in the LaBr detectors is also improved thus reducing the impact of the time-correlated background.

The doubly gated LaBr spectrum, relevant for the analysis of the $5/2^-_1$ state, is shown in Fig. 3(a). Here the LaBr gate is placed on the decay transition. Additionally, doubly gated HPGe spectrum is generated from HPGe-HPGe-LaBr triple coincidences. The high resolution of the HPGe spectrum generated under the same coincidence conditions allows for a check for unwanted contaminant transitions which would not be otherwise resolved by the LaBr scintillators. After placing a second gate in the LaBr spectrum on the feeding transition as indicated in Fig. 3(a) the time difference spectra are generated

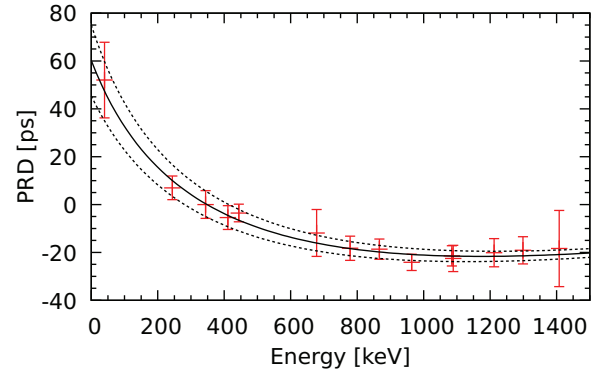

FIG. 2. The fitted PRD of the setup (solid line), together with the data points used to fit the curve. The dashed lines represent the confidence interval corresponding to 1σ standard deviation. The calibration was performed with a ^{152}Eu source.

and displayed in Fig. 3(c). Measuring the centroid difference ΔC between the delayed and the anti-delayed spectra and using Eq. (1), a lifetime of 66(5) ps is obtained. An analogous investigation is performed using the spectra generated when the first LaBr gate is placed on the feeding transition [see Fig. 3(b)]. In both cases, the same two LaBr gates are used resulting in the same time distributions displayed in Fig. 3(c). The background contributions under the full-energy peaks (FEP) of both the feeder and the decay are very low therefore no time-correlated background correction is necessary.

Using the same procedure, the lifetime of the $9/2^-_1$ and the $11/2^-_1$ states were extracted. The corresponding spectra are presented in Figs. 3(d–f) and 3(g–i), respectively. Even though, all the spectra are very clean there is a small background contribution under the 195-keV transition ($11/2^-_1 \rightarrow 9/2^-_1$). In this case the measured the centroid difference ΔC cannot be used directly for determining the lifetimes since it contains contributions from the time-correlated Compton background which comes from the counts underneath the full energy peaks (FEP's). A correction for these contributions can be done by sampling the time response of the background at several positions on either side of the FEP of the decay transition [34]. The data points are then fitted and extrapolated to the position of the FEP to obtain the response of the background under the decay peak ΔC_d^{bg}. The same procedure is applied for the background around the FEP of the feeding transition to obtain ΔC_f^{bg}. The correction to the measured centroid ΔC_{exp} difference is applied according to the formula [34]

$$\Delta C = \Delta C_{\text{exp}} + \Delta C_{\text{corr}},$$
$$\Delta C_{\text{corr}} = \frac{\left(\Delta C_{\text{exp}} - \Delta C_d^{\text{bg}}\right)(p/b)_f^2 + \left(\Delta C_{\text{exp}} - \Delta C_f^{\text{bg}}\right)(p/b)_d^2}{(p/b)_d(p/b)_f[(p/b)_d + (p/b)_f]}, \tag{3}$$

where $(p/b)_d$ and $(p/b)_f$ are the peak to background ratios of the feeding and the decay peaks, respectively. Since the peak to background ratios of the $9/2^-_1 \rightarrow 5/2^-_1$ and the $9/2^+_1 \rightarrow 11/2^-_1$ are larger no correction is needed for the background under these peaks. The correction to the measured centroid

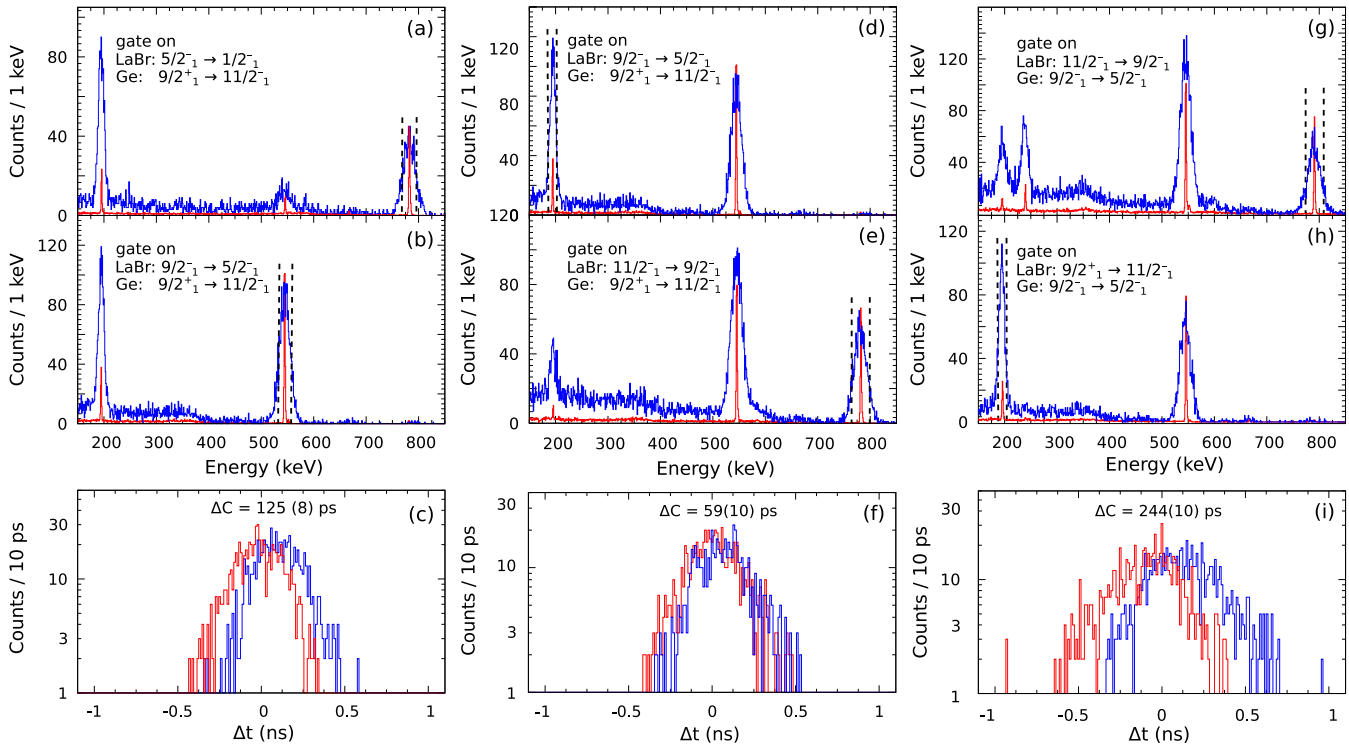

FIG. 3. (a) LaBr (blue) and HPGe (red) detector projections in HPGe-LaBr gates, where the gate in the LaBr spectrum is set on the decay transition. The vertical dashed lines indicate the gates used to produce the time difference spectra displayed in (c). (b) same as (a) but the LaBr gate is set on the feeding transition. (c) Time-difference spectra for the 782-545 keV used to extract the lifetime of the $5/2_1^-$ state. (d), (e), (f) and (g), (h), (i) represent data taken as in (a), (b), (c) but used to extract the lifetimes of the $9/2_1^-$ and the $11/2_1^-$ states, respectively.

difference can be than simplified to

$$\Delta C_{\rm corr} = \frac{\Delta C_{\rm exp} - \Delta C^{\rm bg}}{p/b}, \tag{4}$$

where $\Delta C^{\rm bg}$ and (p/b) refer the $11/2_1^- \rightarrow 9/2_1^-$ transition, which for the $9/2_1^-$ state is a feeding transition while for the $11/2_1^-$ state is a decay transition. In both cases the background correction is about 4 ps. After applying the corrections to the measured centroid differences, the lifetimes of the $9/2_1^-$ and the $11/2_1^-$ states were extracted by using Eq. (1) to be 26(6) ps and 97(6) ps, respectively.

The final results for the lifetimes are summarized in Table I, together with the resulting transition strengths. The present result for the lifetime of the $11/2_1^-$ state agrees well with the previous measurement, while the result for the lifetime of the $5/2_1^-$ state is about 35% shorter than the adopted value [21]. Both present results for the lifetimes of the $11/2_1^-$ and $5/2_1^-$ the state have significantly improved precision in respect to the previous measurement [21]. This is due to the cleaner selection of the "start" and the "stop" signals in the fast-timing techniques which is allowed by the recent technological development of fast $LaBr_3$(Ce) scintillator detectors with high energy resolution [28]. It has to be noted that there is a certain ambiguity for the value of the multipole mixing ratio of the 195-keV ($11/2_1^- \rightarrow 9/2_1^-$) transition. The value adopted in Ref. [31] is based on α_K electron conversion coefficients [21,22], while a smaller value results form a γ-ray angular distribution measurement from an oriented source [35]. A precise determination of multipole mixing ratios which are close to zero is a difficult task and measurements based on electron conversion coefficients are in general more reliable. However, in the particular case of 195-keV transition, it has to be noted that the α_L electron conversion coefficient reported in [22] also indicates that this transition is a pure $M1$. Therefore, we have included in Table I the transitions strengths extracted with both values of the multipole mixing ratio of 195-keV transition. As can be seen, the multipole mixing ratio strongly affects the results for the $B(E2)$ strength of the 195-keV transition while all other transition strengths, including the $B(M1)$ ones, remain virtually intact.

III. DISCUSSION

In order to check to what extent the experimental data in Table I complies with the widely accepted view that the low-lying states of ^{209}Po arise from a weak coupling of a single neutron hole to the excited states of ^{210}Po [21], we have performed a realistic shell-model calculation. Moreover, the comparison between calculated and experimental data, especially the ones on the absolute transition strengths, also serves to test the reliability and the limits of the adopted Hamiltonian. The calculations have been performed using the code KSHELL [36], by assuming ^{208}Pb as a closed inert core, while the valence proton particles and neutron holes are left to occupy the orbitals $2p_{3/2}, 2p_{1/2}, 1f_{7/2}, 1f_{5/2}, 0h_{9/2}, 0i_{13/2}$ which are labeled with nlj, n starting from 0. The proton single-particle and neutron single-hole energies of the shell-model effective

TABLE I. Properties of the three investigated low-lying states of ^{209}Po and the γ-ray transitions originating from their decays.

E_{level} (keV)	J_i^π	J_f^π	E_γ (keV)	I_γ[a] (%)	α[b]	δ	$\tau_{(lit.)}$[c] (ps)	τ[d] (ps)	Transition strength[d,e] $J_i^\pi \to J_f^\pi$
545	$5/2_1^-$						101(29)	66(5)	
		$1/2_1^-$	545	100	0.0262				$B(E2) = 251^{+21}_{-18}$
1327	$9/2_1^-$							26(6)	
		$5/2_1^-$	782	100(3)	0.0120				$B(E2) = 106^{+32}_{-20}$
		$5/2_2^-$	151	0.097(18)	1.319				$B(E2) = 378^{+139}_{-96}$
1522	$11/2_1^-$						101(29)	97(6)	
		$9/2_1^-$	195	100(5)	1.51(13)	$+0.40^{+0.17}_{-0.22}$[f]			$B(M1) = 0.019(3)$
									$B(E2) = 1129^{+893}_{-718}$
					1.66(3)	0.077(55)[g]			$B(M1) = 0.021(2)$
									$B(E2) = 46^{+79}_{-39}$
		$7/2_1^-$	113	0.78(16)	4.29				$B(E2) = 977^{+226}_{-211}$[h]
									$B(E2) = 937^{+213}_{-201}$[i]
		$13/2_1^-$	104	10.1(16)	9.87				$B(M1) = 0.014(2)$[h]
									$B(M1) = 0.014(2)$[i]

[a]Relative γ-ray intensities. From Ref. [31] and references therein.
[b]Theoretical total internal conversion coefficients. From Ref. [31] and references therein.
[c]From Ref. [21].
[d]From the present work.
[e]$B(E2)$ values are given in $e^2\text{fm}^4$ (1 W.u. = 73.67 $e^2\text{fm}^4$), and $B(M1)$ values are given in μ_N^2.
[f]The adopted multipole mixing ratios. From Ref. [31].
[g]The multipole mixing ratio from Ref. [35].
[h]The value is calculated in the case when the multipole mixing ratio and the total conversion coefficient of the 195-keV transition are adopted to be $+0.40^{+0.17}_{-0.22}$ and 1.51(13), respectively.
[i]The value is calculated in the case when the multipole mixing ratio and the total conversion coefficient of the 195-keV transition are adopted to be +0.077(55) and 1.66(3), respectively.

Hamiltonian have been taken from the experimental spectra of ^{209}Bi [31] and ^{207}Pb [37], and are reported in Table II.

As regards the two-body effective interaction, the proton-proton, neutron-neutron, and proton-neutron matrix elements have been derived, respectively, in the particle-particle, hole-hole, and particle-hole formalism by mean of the $\hat{Q}$ box folded-diagram approach [38,39]. In particular, we have used the perturbative diagrammatic expansion of the $\hat{Q}$ box by including one- and two-body diagrams up to second order in the interaction. The starting point of this procedure is the CD-Bonn nucleon-nucleon potential [40] renormalized by means of the $V_{\text{low-k}}$ approach [41] with a cutoff parameter $\Lambda = 2.2$ fm^{-1}. The Coulomb potential is also taken into account for the proton-proton interaction.

It is worth mentioning that this Hamiltonian was already used in the past, even if with a slightly smaller cutoff parameter ($\Lambda = 2.1$ fm^{-1}), to study the particle-hole multiplets in ^{208}Bi [42]. It was shown that the three experimental multiplets $\pi 0h_{9/2}\nu 2p_{1/2}^{-1}$, $\pi 0h_{9/2}\nu 1f_{5/2}^{-1}$, and $\pi 0h_{9/2}\nu 0i_{13/2}^{-1}$ are well reproduced by theory with an accuracy within 100 keV.

TABLE II. Proton single-particle and neutron single-hole energies adopted in the calculation.

$\pi(nlj)$	ϵ (keV)	$\nu(nlj)^{-1}$	ϵ (keV)
$0h_{9/2}$	0	$2p_{1/2}$	0
$1f_{7/2}$	896	$1f_{5/2}$	570
$0i_{13/2}$	1608	$2p_{3/2}$	898
$1f_{5/2}$	2826	$0i_{13/2}$	1633
$2p_{3/2}$	3118	$1f_{7/2}$	2340
$2p_{1/2}$	3633	$0h_{9/2}$	3415

Experimental and calculated spectra of ^{209}Po are shown in Fig. 4, where we have reported energy levels up to 1.6 MeV. The calculated excitation energies are in a very good agreement with the experimental data, discrepancies being less than 110 keV for almost all the states.

The calculated wave functions were used to compute the transition probabilities and moments that are compared with

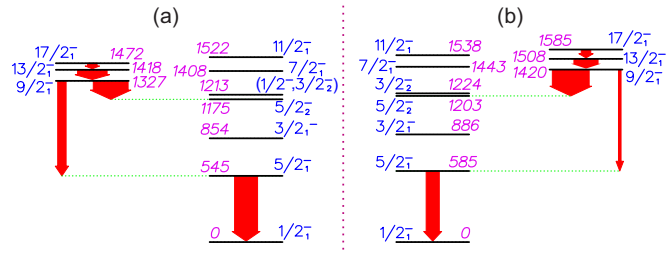

FIG. 4. Comparison of experimental low-lying negative-parity excited states of ^{209}Po (a) with the calculated ones (b) (for details see the text). The experimental data are taken from Ref. [31]. The energies of the levels are given in keV. The arrows represent some of the transitions discussed the text. The widths of the arrows are proportional to the absolute $E2$ transition strengths.

TABLE III. Calculated and experimental reduced transition probabilities and moments in ^{209}Po. The $B(E2)$ values are given in $e^2\text{fm}^4$, the quadrupole moments are in $e\text{fm}^2$, the magnetic moments are in μ_N and $B(M1)$ in μ_N^2.

Quantity	Calculated value	Experimental value[a]
$\mu(1/2_1^-)$	+0.31	+0.61(5)
$\mu(13/2_1^-)$	+6.05	+6.13(9)
$\mu(17/2_1^-)$	+7.84	+7.75(5)
$Q(13/2_1^-)$	−12.6	|12.6(5)|
$Q(17/2_1^-)$	−64.4	|65.9(7)|
$B(E2;5/2_1^- \to 1/2_1^-)$	142	251^{+21}_{-18}[b]
$B(E2;9/2_1^- \to 5/2_2^-)$	404	378^{+139}_{-96}[b]
$B(E2;9/2_1^- \to 5/2_1^-)$	29	106^{+32}_{-20}[b]
$B(E2;13/2_1^- \to 9/2_1^-)$	276	322(7)
$B(E2;17/2_1^- \to 13/2_1^-)$	104	105(4)
$B(M1;11/2_1^- \to 13/2_1^-)$	0.012	0.014(2)[b,c,d]
$B(E2;11/2_1^- \to 7/2_1^-)$	262	977^{+226}_{-211}[b,c]
		937^{+213}_{-201}[b,c]
$B(E2;11/2_1^- \to 9/2_1^-)$	10	1129^{+893}_{-718}[b,c]
		46^{+79}_{-39}[b,d]
$B(M1;11/2_1^- \to 9/2_1^-)$	0.010	0.019(3)[b,d]
		0.021(2)[b,d]

[a]The data are taken from Ref. [31] unless otherwise stated.
[b]From the present work.
[c]The value is calculated in the case when the multipole mixing ratio and the total conversion coefficient of the 195-keV transition are adopted to be $+0.40^{+0.17}_{-0.22}$ and 1.51(13), respectively (cf. Table I).
[d]The value is calculated in the case when the multipole mixing ratio and the total conversion coefficient of the 195-keV transition are adopted to be +0.077(55) and 1.66(3), respectively (cf. Table I).

the experimental data in Table III. They have been calculated by employing the empirical effective charges $e_\pi = 1.5e$, $e_\nu = 0.92e$, whereas the adopted values for the effective gyromagnetic factors are $g_\pi^l = 1.2$, $g_\nu^l = -0.2$, $g_{\pi,\nu}^s = 0.7(g_{\pi,\nu}^s)_{bare}$. This choice of the effective charges and gyromagnetic factors leads to an overall good description of electromagnetic properties of ^{206}Pb, ^{207}Pb, ^{209}Bi, and ^{210}Po, although we should mention that the predicted $B(E2;2_1^+ \to 0_1^+)$ in ^{210}Po is ≈6.5 times larger then the experimental value reported in Ref. [31] and twice the data reported in Ref. [18] in line with the results of Refs. [8,9,17,43], and the magnetic dipole moments of the yrast $1/2_1^-$ and $5/2_1^-$ states in ^{207}Pb area about half of the measured ones.

It can be seen from Table III that the measured $B(M1;11/2_1^- \to 13/2_1^-)$ is very well reproduced. As regard the $B(M1;11/2_1^- \to 9/2_1^-)$, the calculated value is in quite good agreement with the two very close experimental values corresponding to the two adopted multipole mixing ratios.

On the other hand, the quality of the agreement between theory and experiment for the $B(E2)$'s strongly depends on the involved states. In fact, leaving out the $E2$ transitions from the $11/2_1^-$ state (we shall discuss these cases at the end of the section), the difference between theory and experiment for the other $B(E2)$ values ranges from 1 to about 100 $e^2\text{fm}^4$. As regards the moments, a very good agreement is found for the

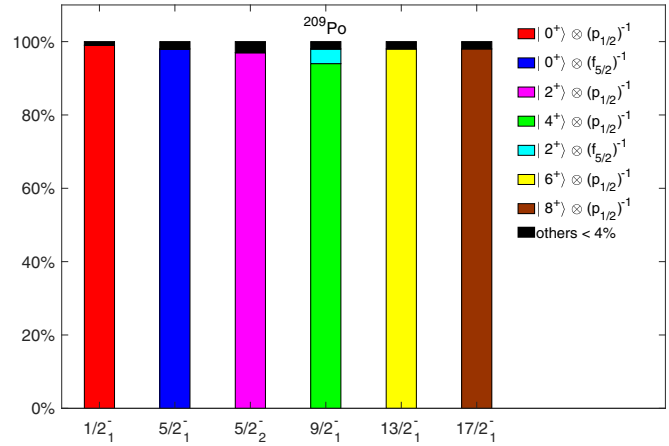

FIG. 5. Composition of selected states in ^{209}Po. See text for details.

$13/2_1^-$ and $17/2_1^-$ states, while the magnetic dipole moment of the $1/2_1^-$ state is underestimated by a factor ≈2.

To understand the reasons of these discrepancies we have analyzed the composition of the wave functions of ^{209}Po, by writing them in terms of a neutron hole coupled to the states of ^{210}Po. In Fig. 5, we report the components of such a development together with their probability amplitudes (>4%) for the $1/2_1^-$, $5/2_{1,2}^-$, $9/2_1^-$, $13/2_1^-$, and $17/2_1^-$ states. These amplitudes are strictly related to the one neutron pick-up spectroscopic factors from ^{210}Po, which are reported in Table IV for the sake of completeness.

All these states are characterized by a dominant component accounting for 94–99% of the calculated wave functions. In particular, the first $1/2^-$ and $5/2^-$ states are of single-hole nature resulting from the coupling of a $2p_{1/2}$ and $1f_{5/2}$ neutron hole, respectively, to the ground state of ^{210}Po. On the other hand, the other states arise mainly from $|\pi J^\pi \neq 0^+\rangle \otimes (\nu 2p_{1/2})^{-1}$ configurations, with $J^\pi = 2^+, 4^+, 6^+, 8^+$ for the $5/2_2^-$, $9/2_1^-$, $13/2_1^-$, $17/2_1^-$ states, respectively.

For each $E2$ transition involving these states, we have calculated the $|\langle J_f||E2||J_i\rangle|$ matrix element by including only the dominant component of the initial and final wave functions. Their values are shown (in blue) in Fig. 6, where we have also reported the remaining contributions (in green) due to the presence of minor components in the wave functions together with the experimental data (in red). The percentages of the two

TABLE IV. One neutron pick-up spectroscopic factors from ^{210}Po for selected states in ^{209}Po.

J_f^π	(nlj)	J_i^π	C^2S
$1/2_1^-$	$2p_{1/2}$	0_1^+	1.982
$5/2_1^-$	$1f_{5/2}$	0_1^+	5.863
$5/2_2^-$	$2p_{1/2}$	2_1^+	1.158
$9/2_1^-$	$2p_{1/2}$	4_1^+	1.048
	$1f_{5/2}$	2_1^+	0.085
$13/2_1^-$	$2p_{1/2}$	6_1^+	1.056
$17/2_1^-$	$2p_{1/2}$	8_1^+	1.034

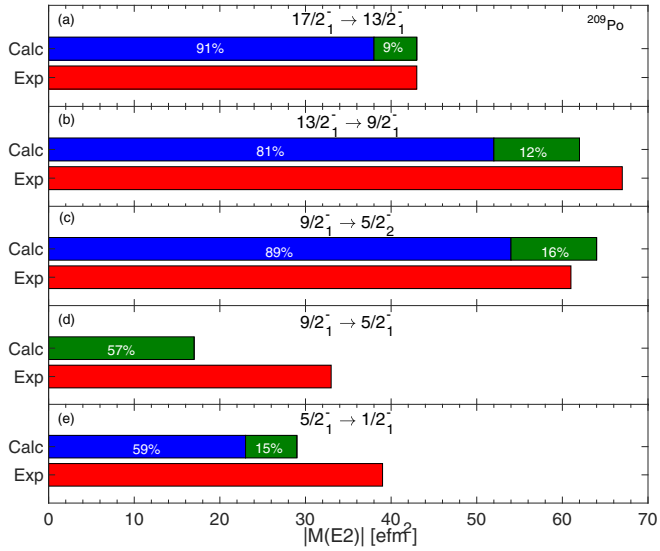

FIG. 6. Calculated and experimental $|\langle J_f||E2||J_i\rangle|$ matrix elements. For each $E2$ transition, the blue bar represents the contribution from the dominant component of the initial and final wave function, while the green bar the remaining one. The percentages refer to experimental data.

calculated contributions relative to the experimental values are also indicated.

A first observation is that the $B(E2; 17/2^-_1 \rightarrow 13/2^-_1)$, $B(E2; 13/2^-_1 \rightarrow 9/2^-_1)$, and $B(E2; 9/2^-_1 \rightarrow 5/2^-_2)$ strengths, for which we obtain a good agreement, are mostly determined by the transitions between the dominant components of the involved states. It turns out that 91%, 81%, and the 89% of the experimental value of these three $B(E2)$'s is covered, respectively, by the $|\pi 8^+\rangle \otimes (\nu p_{1/2})^{-1} \rightarrow |\pi 6^+\rangle \otimes (\nu p_{1/2})^{-1}$, $|\pi 6^+\rangle \otimes (\nu p_{1/2})^{-1} \rightarrow |\pi 4^+\rangle \otimes (\nu p_{1/2})^{-1}$, and $|\pi 4^+\rangle \otimes (\nu p_{1/2})^{-1} \rightarrow |\pi 2^+\rangle \otimes (\nu p_{1/2})^{-1}$ transition. Clearly, each of these three transitions only contributes through the proton term, namely through the corresponding transition in ^{210}Po.

For the other two $B(E2)$ strengths in ^{209}Po, i.e., $B(E2; 9/2^-_1 \rightarrow 5/2^-_1)$, $B(E2; 5/2^-_1 \rightarrow 1/2^-_1)$, the dominant components of the wave functions play a minor role. As a matter of fact, no contribution is given to the $B(E2; 9/2^-_1 \rightarrow 5/2^-_1)$ by the transition $|\pi 4^+\rangle \otimes (\nu p_{1/2})^{-1} \rightarrow |\pi 0^+\rangle \otimes (\nu f_{5/2})^{-1}$, while the $|\pi 0^+\rangle \otimes (\nu f_{5/2})^{-1} \rightarrow |\pi 0^+\rangle \otimes (\nu p_{1/2})^{-1}$ transition accounts only for 57% of the experimental $B(E2; 5/2^-_1 \rightarrow 1/2^-_1)$ value. On the other hand, the minor components of the $1/2^-_1$, $5/2^-_1$, $9/2^-_1$ wave functions do not give the required additional strength to reproduce the experimental $B(E2)$ values.

An increase of components other the dominant one is needed to reduce discrepancies with experiment. We have verified, for instance, that a few percentage increase of about 4–5% of the $|\pi 2^+\rangle \otimes (\nu f_{5/2})^{-1}$ component in the $1/2^-_1$ and $9/2^-_1$ states and the $|\pi 2^+\rangle \otimes (\nu p_{1/2})^{-1}$ component in the $5/2^-_1$ state, is able to lead to the correct $B(E2; 9/2^-_1 \rightarrow 5/2^-_1)$, $B(E2; 5/2^-_1 \rightarrow 1/2^-_1)$ values and, also to improve the agreement for the $B(E2; 9/2^-_1 \rightarrow 5/2^-_2)$.

This is a clear signature that our calculations predict a too small percentage of components other than the dominant one. In other words, although these calculations give a quite reasonable account of the main features of the ^{209}Po wave functions, they are not able to produce the needed configuration mixing. This finding points to some uncertainty in the determinations of the off-diagonal matrix elements of the adopted proton-neutron effective interaction. Therefore, a fine tuning of the latter would be needed to improve the agreement with experiment.

It is worth noting, however, that the reduced fragmentation predicted by our calculations cannot account for the discrepancy we find between theory and experiment for the magnetic dipole moment of the $1/2^-_1$ state as well as for the two $E2$ transitions from the $11/2^-_1$ state. For the magnetic moment, the discrepancy is expected to arise also from the underestimation of the corresponding moment in ^{207}Pb, as mentioned above. The deficiencies in describing the magnetic moments of ground states of ^{209}Po and ^{207}Pb, as well as the overestimation of the $B(E2; 2^+_1 \rightarrow 0^+_1)$ in ^{210}Po, may be related to core-excited components of the ^{208}Pb core, which are outside the used model space and are not completely accounted for by the effective charges and effective g factors. This is also the case when using the Kuo-Herling interaction [12] and has recently been discussed with respect to $B(E2; 2^+_1 \rightarrow 0^+_1)$ in ^{210}Po [43].

Our predicted value for the $B(E2; 11/2^-_1 \rightarrow 7/2^-_1)$ differs from the possible experimental values (cf. Table III) by about 700 e^2fm^4, which seems to indicate a more serious lack in our wave functions. The $11/2^-_1$ and $7/2^-_1$ states, as those reported in Fig. 5, are characterized by a single main component, namely $|\pi 6^+\rangle \otimes (\nu 2p_{1/2})^{-1}$ and $|\pi 4^+\rangle \otimes (\nu 2p_{1/2})^{-1}$, and a small increase in the weight of the minor components cannot provide the so large missing contributions. Moreover, the same big discrepancies between theoretical and experimental B($E2$)'s from the $11/2^-_1$ state were found in Ref. [17], where shell-model calculations were performed for several nuclei of this region adopting a phenomenological Hamiltonian. On this basis, a remeasurement of this transition, which is affected by a large error, is certainly required. As for the $11/2^-_1 \rightarrow 9/2^-_1$ transition, the ambiguity on the multipole mixing ratio gives rise to two very different values of the $B(E2)$ (cf. Table III). The very large $B(E2)$ value corresponding to $\delta = +0.40$ implies a more substantial change in our predicted wave functions than that discussed for the $11/2^-_1 \rightarrow 7/2^-_1$ transition. The other δ value leads to a $B(E2)$ strength whose value is only 30 e^2fm^4 larger than that predicted by theory and, consistently with the analysis made for the other transitions, can be explained by a small additional configuration mixing.

IV. SUMMARY

In the present study we have measured the lifetimes of the $11/2^-_1$, the $9/2^-_1$ and the $5/2^-_1$ states of ^{209}Po. The derived absolute $M1$ and $E2$ transition strengths together with the previously available experimental data on the low-lying negative-parity states of ^{209}Po have been compared to results of shell-model calculations with a realistic effective interaction

derived from the CD-Bonn nucleon-nucleon potential within the framework of $\hat{Q}$ box folded-diagram approach.

The experimental excitation energies of the low-lying negative states of ^{209}Po are very well reproduced by theory, while the agreement for the electromagnetic properties is less satisfactory. It turns out, in fact, that the quality of agreement, especially for the $B(E2)$'s, depends on the involved states. This may be seen as a clear indication of some deficiency inherent in the structure of our calculated wave functions. We predict that the low-lying negative-parity states of ^{209}Po are dominated by the coupling of a neutron hole to the yrast states of ^{210}Po, which implies that the removal of one neutron from the ^{210}Po does not induce any additional quadrupole collectivity. A detailed analysis of the $B(E2)$ transitions confirms this finding, although it also suggests that we underestimate the weight of the minor components of the wave functions. We have verified that a few percentage increase of these components is required to obtain a quantitative description of all transition strengths. The presence of such a small but apparently essential configuration mixing clearly evidences the role of the proton-neutron part of the effective interaction and the need of a fine tuning of its matrix elements.

ACKNOWLEDGMENTS

We thank H. Naïdja and S. Dimitrova for the fruitful discussions. M.S. acknowledges the support by the Bulgarian Ministry of Education and Science under the National Research Program Young scientists and post-doctoral students RD-22-844. G.DeG. and A.G. acknowledge the CINECA award under the ISCRA initiative and through the INFN-CINECA agreement for the availability of high performance computing resources and support. G.DeG. acknowledges also the support by the funding program "VALERE" of Universitá degli Studi della Campania "Luigi Vanvitelli". This work was supported by the DAAD partnership agreement between the University of Cologne and University of Sofia, and by the Bulgarian National Science Fund under Grant No. DN08/23/2016.

[1] M. G. Mayer, Phys. Rev. **75**, 1969 (1949).
[2] O. Haxel, J. H. D. Jensen, and H. E. Suess, Phys. Rev. **75**, 1766 (1949).
[3] R. F. Casten, Phys. Lett. B **152**, 145 (1985).
[4] A. de Shalit and I. Talmi, *Nuclear Shell Theory* (Academic Press, New York, 1963).
[5] J. B. Mcgrory and T. T. S. Kuo, Nucl. Phys. A **247**, 283 (1975).
[6] C. W. Ma and W. W. True, Phys. Rev. C **8**, 2313 (1973).
[7] D. Zwarts and P. W. M. Glaudemans, Z. Phys. A **320**, 487 (1985).
[8] T. R. McGoram, G. D. Dracoulis, A. P. Byrne, A. R. Poletti, and S. Bayer, Nucl. Phys. A **637**, 469 (1998).
[9] L. Coraggio, A. Covello, A. Gargano, N. Itaco, and T. T. S. Kuo, Phys. Rev. C **58**, 3346 (1998).
[10] L. Coraggio, A. Covello, A. Gargano, N. Itaco, and T. T. S. Kuo, Phys. Rev. C **60**, 064306 (1999).
[11] E. Caurier, M. Rejmund, and H. Grawe, Phys. Rev. C **67**, 054310 (2003).
[12] E. K. Warburton and B. A. Brown, Phys. Rev. C **43**, 602 (1991).
[13] B. Silvestre-Brac and J. P. Boisson, Phys. Rev. C **24**, 717 (1981).
[14] L. Rydstrom, J. Blomqvist, R. J. Liotta, and C. Pomar, Nucl. Phys. A **512**, 217 (1990).
[15] A. Zemel and J. Dobes, Phys. Rev. C **27**, 2311 (1983).
[16] Z. Y. Xu, Y. Lei, Y. M. Zhao, S. W. Xu, Y. X. Xie, and A. Arima, Phys. Rev. C **79**, 054315 (2009).
[17] E. Teruya, K. Higashiyama, and N. Yoshinaga, Phys. Rev. C **93**, 064327 (2016), and references therein.
[18] D. Kocheva, G. Rainovski, J. Jolie, N. Pietralla, A. Blazhev, A. Astier, T. Braunroth, M. L. Cortés, A. Dewald, M. Djongolov, C. Fransen, K. Gladnishki, A. Hennig, V. Karayonchev, J. M. Keatings, J. Litzinger, C. Müller-Gatermann, P. Petkov, M. Scheck, P. Spagnoletti, P. Scholz, C. Stahl, R. Stegmann, M. Stoyanova, P. Thöle, N. Warr, V. Werner, W. Witt, D. Wölk, K. O. Zell, P. Van Isacker, and V. Yu. Ponomarev, Eur. Phys. J. A **53**, 175 (2017).
[19] M. Stoyanova, G. Rainovski, J. Jolie, N. Pietralla, A. Blazhev, M. Beckers, A. Dewald, M. Djongolov, A. Esmaylzadeh, C. Fransen, L. M. Gerhard, K. A. Gladnishki, S. Herb, P. R. John, V. Karayonchev, J. M. Keatings, R. Kern, L. Knafla, D. Kocheva, L. Kornwebel, T. Kröll, M. Ley, K. M. Mashtakov, C. Müller-Gatermann, J.-M. Régis, M. Scheck, K. Schomacker, J. Sinclair, P. Spagnoletti, C. Sürder, N. Warr, V. Werner, and J. Wiederhold, Phys. Rev. C **100**, 064304 (2019).
[20] T. J. Gray, J. M. Allmond, A. E. Stuchbery, C.-H. Yu, C. Baktash, A. Gargano, A. Galindo-Uribarri, D. C. Radford, J. C. Batchelder, J. R. Beene, C. R. Bingham, L. Coraggio, A. Covello, M. Danchev, C. J. Gross, P. A. Hausladen, N. Itaco, W. Krolas, J. F. Liang, E. Padilla-Rodal, J. Pavan, D. W. Stracener, and R. L. Varner, Phys. Rev. Lett. **124**, 032502 (2020).
[21] M. Alpsten, Å. Appelqvist, and G. Astner, Phys. Scr. **4**, 137 (1971).
[22] L. J. Jardine, S. G. Prussin, and J. M. Hollander, Nucl. Phys. A **233**, 25 (1974).
[23] T. Yamazaki and E. Matthias, Phys. Rev. **175**, 1476 (1968).
[24] O. Häusser, T. K. Alexander, J. R. Beene, E. D. Earle, A. B. McDonald, F. C. Khanna, and I. S. Towner, Nucl. Phys. A **273**, 253 (1976).
[25] W. Baldridge, N. Freed, and J. Gibbons, Phys. Lett. B **36**, 179 (1971).
[26] G. Nicolescu, E. A. Ivanov, and D. Plostinaru, Phys. Rev. C **79**, 044314 (2009).
[27] J.-M. Régis, G. Pascovici, J. Jolie, and M. Rudigier, Nucl. Instrum. Methods Phys. Res. A **622**, 83 (2010).
[28] A. Iltis, M. R. Mayhugh, P. Menge, C. M. Rozsa, O. Selles, and V. Solovyev, Nucl. Instrum. Methods Phys. Res. A **563**, 359 (2006).
[29] J.-M. Régis, N. Saed-Samii, M. Rudigier, S. Ansari, M. Dannhoff, A. Esmaylzadeh, C. Fransen, R.-B. Gerst, J. Jolie, V. Karayonchev, C. Müller-Gatermann, and S. Stegemann, Nucl. Instrum. Methods Phys. Res. A **823**, 72 (2016).

[30] Pragati, A. Y. Deo, Z. Podolyák, P. M. Walker, A. Algora, B. Rubio, J. Agramunt, L. M. Fraile, N. Al-Dahan, N. Alkhomashi, J. A. Briz, M. E. Estevez Aguado, G. Farrelly, W. Gelletly, A. Herlert, U. Köster, and A. Maira, Phys. Rev. C **94**, 064316 (2016).
[31] J. Chen and F. G. Kondev, Nucl. Data Sheets **126**, 373 (2015).
[32] J.-M. Régis, H. Mach, G. S. Simpson, J. Jolie, G. Pascovici, N. Saed-Samii, N. Warr, A. Bruce, J. Degenkolb, L. M. Fraile, C. Fransen, D. G. Ghita, S. Kisyov, U. Koester, A. Korgul, S. Lalkovski, N. Mărginean, P. Mutti, B. Olaizola, Z. Podolyak, P. H. Regan, O. J. Roberts, M. Rudigier, L. Stroe, W. Urban, and D. Wilmsen, Nucl. Instrum. Methods Phys. Res. A **726**, 191 (2013).
[33] J.-M. Régis, M. Rudigier, J. Jolie, A. Blazhev, C. Fransen, G. Pascovici, and N. Warr, Nucl. Instrum. Methods Phys. Res. A **684**, 36 (2012).
[34] J.-M. Régis, A. Esmaylzadeh, J. Jolie, V. Karayonchev, L. Knafla, U. Köster, Y. H. Kim, and E. Strub, Nucl. Instrum. Methods Phys. Res. A **955**, 163258 (2020).
[35] P. Šimeček, I. Procházka, Chan Kim Kchung, M. Finger, M. I. Fominykh, B. A. Gvozdev, A. P. Kabachenko, T. Lešner, P. Malinský, V. N. Pavlov, and M. Vobecký, Hyperfine Interact. **34**, 131 (1987).
[36] N. Shimizu, T. Mizusaki, T. Utsuno, and Y. Tsunoda, Comput. Phys. Commun. **244**, 372 (2019).
[37] F. G. Kondev and S. Lalkovski, Nucl. Data Sheets **112**, 707 (2011).
[38] L. Coraggio, A. Covello, A. Gargano, N. Itaco, and T. T. S. Kuo, Prog. Part. Nucl. Phys. **62**, 135 (2009).
[39] L. Coraggio, A. Covello, A. Gargano, N. Itaco, and T. T. S. Kuo, Ann. Phys. (NY) **327**, 2125 (2012).
[40] R. Machleidt, Phys. Rev. C **63**, 024001 (2001).
[41] S. Bogner, T. T. S. Kuo, and L. Coraggio, Nucl. Phys. A **684**, 432c (2001).
[42] A. Covello, L. Coraggio, A. Gargano, and N. Itaco, Phys. At. Nucl. **67**, 1611 (2004).
[43] V. Karayonchev, A. Blazhev, A. Esmaylzadeh, J. Jolie, M. Dannhoff, F. Diel, F. Dunkel, C. Fransen, L. M. Gerhard, R.-B. Gerst, L. Knafla, L. Kornwebel, C. Müller-Gatermann, J.-M. Régis, N. Warr, K. O. Zell, M. Stoyanova, and P. Van Isacker, Phys. Rev. C **99**, 024326 (2019).